Large-scale BAO signatures of the smallest galaxies

Dalal, N ; Pen, U L ; Seljak, U

Abstract: Recent work has shown that at high redshift, the relative velocity between dark matter and baryonic gas is typically supersonic. This relative velocity suppresses the formation of the earliest baryonic structures like minihalos, and the suppression is modulated on large scales. This effect imprints a characteristic shape in the clustering power spectrum of the earliest structures, with significant power on 100 Mpc scales featuring highly pronounced baryon acoustic oscillations. The amplitude of these oscillations is orders of magnitude larger at z 20 than previously expected. This characteristic signature can allow us to distinguish the effects of minihalos on intergalactic gas at times preceding and during reionization. We illustrate this effect with the example of 21 cm emission and absorption from redshifts during and before reionization. This effect can potentially allow us to probe physics on kpc scales using observations on 100 Mpc scales. We present sensitivity forecasts for FAST and Arecibo. Depending on parameters, this enhanced structure may be detectable by Arecibo at z 15-20, and with appropriate instrumentation FAST could measure the BAO power spectrum with high precision. In principle, this effect could also pose a serious challenge for efforts to constrain dark energy using observations of the BAO feature at low redshift.

DOI: https://doi.org/10.1088/1475-7516/2010/11/007

Draft version September 27, 2010
Preprint typeset using LaTeX style emulateapj v. 8/13/10

LARGE-SCALE BAO SIGNATURES OF THE SMALLEST GALAXIES

Neal Dalal and Ue-Li Pen
Canadian Institute for Theoretical Astrophyics, University of Toronto, 60 St. George St., Toronto, Ontario M5S 3H8, Canada

Uros Seljak
Physics Department and Lawrence Berkeley National Laboratory, University of California, Berkeley, California 94720, USA
Institute for Theoretical Physics, University of Zurich, Zurich, Switzerland and
Institute for Early Universe, Ewha University, Seoul 120-750, S. Korea
Draft version September 27, 2010

ABSTRACT

Recent work has shown that at high redshift, the relative velocity between dark matter and baryonic gas is typically supersonic. This relative velocity suppresses the formation of the earliest baryonic structures like minihalos, and the suppression is modulated on large scales. This effect imprints a characteristic shape in the clustering power spectrum of the earliest structures, with significant power on ∼100 Mpc scales featuring highly pronounced baryon acoustic oscillations. The amplitude of these oscillations is orders of magnitude larger at $z \sim 20$ than previously expected. This characteristic signature can allow us to distinguish the effects of minihalos on intergalactic gas at times preceding and during reionization. We illustrate this effect with the example of 21 cm emission and absorption from redshifts during and before reionization. This effect can potentially allow us to probe physics on kpc scales using observations on 100 Mpc scales.

We present sensitivity forecasts for FAST and Arecibo. Depending on parameters, this enhanced structure may be detectable by Arecibo at $z \sim 15 - 20$, and with appropriate instrumentation FAST could measure the BAO power spectrum with high precision. In principle, this effect could also pose a serious challenge for efforts to constrain dark energy using observations of the BAO feature at low redshift.

1. INTRODUCTION

Structure formation in the standard inflationary Λ-Cold Dark Matter (ΛCDM) cosmological model is expected to proceed hierarchically. The earliest bound, virialized structures arise on small scales, and as time progresses these objects merge and accrete mass, growing ever larger until cosmic acceleration at low redshift freezes out the growth of large-scale structure.

The role played by the earliest generations of collapsed structures in the thermal history of the universe is, at present, unclear. Observations of the spectra of high-redshift quasars indicate that the reionization of the intergalactic medium was largely complete by redshift $z \approx 7$ (e.g. Fan et al. 2006), while measurements of the Thomson scattering optical depth of the cosmic microwave background suggest that reionization occurred at $z \sim 10$ (Larson et al. 2010). At these epochs, the typical masses of collapsed dark matter halos range from rare $10^9 M_\odot$ objects, down to (plausibly) Earth-mass halos (Green et al. 2005). As we discuss below, the smallest dark matter halos are unable to attract baryons, resulting in an effective lower mass limit near $10^5 M_\odot$.

Even if low-mass halos are able to acquire baryons, they may be unable to convert those baryons into stars (Tegmark et al. 1997; Bromm et al. 2009; Loeb 2010), since star formation requires the presence of cold, dense gas. Objects massive enough to attract gas but whose virial temperatures are below $\sim 10^4$ K, termed minihalos, cannot cool their gas through atomic lines and must therefore rely upon molecular cooling processes. It is unclear whether molecular processes can cool minihalo gas sufficiently to allow star formation. Prior to the formation of the first stars in the Universe, the formation of molecular H_2 catalyzed by residual free electrons left over after recombination appears insufficient to allow efficient cooling at redshifts $z \lesssim 20$ (Tegmark et al. 1997). However, feedback from the first luminous objects can change this result. Positive feedback, for example from ionizing X-rays that strip electrons from atoms and thereby spur molecule creation, could lead to efficient cooling. Conversely, negative feedback in the form of ultraviolet radiation in the Lyman and Werner bands could destroy molecules and suppress H_2 cooling over large volumes (Yoshida et al. 2007). Given this wide range of possible scenarios, it is unclear whether minihalos can form stars and whether they might be important during the reionization of the intergalactic medium. This uncertainty, however, may be viewed as an opportunity: any probe that can quantify the importance of minihalos during redshifts preceding and during reionization would dramatically help to elucidate the physics of star formation in the first structures that arise in the Universe.

Recently, Tseliakhovich & Hirata (2010, hereafter TH) pointed out an important effect governing the formation of $\sim 10^5 M_\odot$ minihalos, that had previously been overlooked. As we discuss below, this effect can provide a minihalo signature in many potential observables. TH noticed that the relative velocity between dark matter and baryons following recombination is typically supersonic. This relative velocity arises because dark matter is accelerated by

gravitational potential gradients, while baryons are Jeans stabilized against gravitational collapse due to their tight coupling with the photon radiation field, until recombination. Because DM and baryons suffer different accelerations, they acquire significant relative velocities that are predominantly sourced by potential fluctuations on scales of order the sound horizon at recombination, ~ 150 Mpc. At recombination, the baryon sound speed and Jeans length fall precipitously, allowing baryons to respond to the same gravitational potential wells that accelerate dark matter. Subsequently, the large-scale relative velocity is unsourced and decays as a^{-1} following recombination. At redshifts $z \approx 1000$, the relative DM-baryon motion is highly supersonic, with Mach numbers $\mathcal{M} \approx 5$. The gas sound speed does not initially decay as quickly as a^{-1} because of residual thermal coupling to the CMB, so the Mach number diminishes over time to $\mathcal{M} \sim 2$ at $z \sim 100$, and remains nearly constant thereafter.

Because the relative motions between baryons and DM are supersonic, they have significant effects on the growth of structure. TH computed the effects of relative DM-baryon velocities at high redshift, in the perturbative regime of structure formation. They showed that these motions cause a $\sim 10\%$ suppression of the matter power spectrum at $k \approx 200\mathrm{Mpc}^{-1}$ compared to standard linear perturbation theory calculations. Using a Press-Schechter approach, TH also suggested that the abundance of dark matter halos of mass $M \sim 10^6 M_\odot$ could be suppressed by a factor of ~ 2 at redshift $z = 40$. At later redshifts closer to reionization, $z \approx 10 - 20$, the halo abundance would be much closer to standard predictions.

In this paper, we consider a similar effect of the supersonic relative velocities that TH discussed. Instead of considering the effect on dark matter halos, we examine the impact on baryonic objects, which likely determine the properties of observable quantities like 21 cm absorption, emission, etc. The supersonic flow changes the mass threshold of baryonically populated halos, and this effect can be exponentially large for rare objects. The relative bulk flows between DM and baryons are modulated on large scales, of order ~ 100 Mpc, meaning that the minihalo abundance is similarly modulated. This provides a large-scale signature of the effect of minihalos.

All calculations presented here assume WMAP (Larson et al. 2010) cosmological parameters: $\Omega_m = 0.27$, $\Omega_\Lambda = 0.73$, $\Omega_b = 0.045$, $h = 0.7$, $n_s = 0.96$, $\sigma_8 = 0.8$.

2. BARYONIC COLLAPSE FRACTION

In this section, we compute the statistics of the collapsed baryonic density, which we parametrize using f_c, the collapsed fraction of baryons. The baryonic collapsed fraction is different than the CDM collapsed fraction because baryons, unlike CDM, have a nonzero temperature, and therefore cannot fall into shallow potential wells. Naively, we might expect that the characteristic mass M_c unable to attract baryons would scale like the Jeans mass $M_J \propto c_s^3/GH$, however cosmological hydrodynamic simulations (Gnedin 2000; Naoz et al. 2010) have found instead that M_c scales like the filter scale (Gnedin & Hui 1998),

$$M_F^{2/3} = \frac{3}{a}\int_0^a da' M_J^{2/3}(a')\left[1 - \left(\frac{a'}{a}\right)^{1/2}\right]. \tag{1}$$

For a standard WMAP cosmology, $M_c \sim 2 - 3 \times 10^4 M_\odot$ at $z \sim 20$ (Naoz et al. 2010).

Just as gas pressure impedes the collapse of baryons, we expect that bulk relative velocity between gas and dark matter halos will also suppress the accretion of baryons. We can make a simple estimate of the minimum halo mass that can accrete gas moving at some bulk velocity v relative to the halo through analogy to the above argument. Assuming that bulk kinetic energy is converted into thermal energy when gas falls into the halo, we expect that Eqn. (1) will still hold if we replace the sound speed c_s with $c_{s,\mathrm{eff}} = (c_s^2 + v^2)^{1/2}$. Since c_s and v both scale as a^{-1} (see below), this effectively multiplies the critical mass scale by the factor $(1 + v^2/c_s^2)^{3/2}$.

Given M_c, we can compute the baryon collapsed fraction f_c by integrating the halo mass function,

$$f_c = \bar{\rho}^{-1}\int_{M_c}^\infty M\frac{dn}{dM}dM, \tag{2}$$

where we use the fitting function of Sheth et al. (2001) to describe the halo mass function dn/dM. Since M_c is a function of the local relative velocity between CDM and baryons, $\boldsymbol{v}_{cb} \equiv \boldsymbol{v}_c - \boldsymbol{v}_b$, we see that the collapse fraction f_c is also modulated by this velocity, $f_c(\boldsymbol{x}) = f_c(v_{cb}(\boldsymbol{x}))$. We have assumed that the velocity dependence of the collapse fraction is a sharp cut-off in the mass function, whereas hydrodynamic simulations (e.g. Gnedin 2000; Naoz et al. 2010) find a smooth transition in baryon content of halos below and above M_c. This distinction will not be significant for our results: the important point is that the collapse fraction is now a function of the local relative bulk velocity between dark matter and baryons.

The relative velocity between CDM and baryons can be computed using the linearized continuity equation

$$\dot{\delta} + a^{-1}\nabla\cdot\boldsymbol{v} = 0, \tag{3}$$

using comoving coordinates rather than proper coordinates. In the linear regime, where we have potential flow, the velocity is

$$\boldsymbol{v}(\boldsymbol{k}, a) = -i\frac{a\boldsymbol{k}}{k^2}\dot{\delta}(\boldsymbol{k}, a)$$

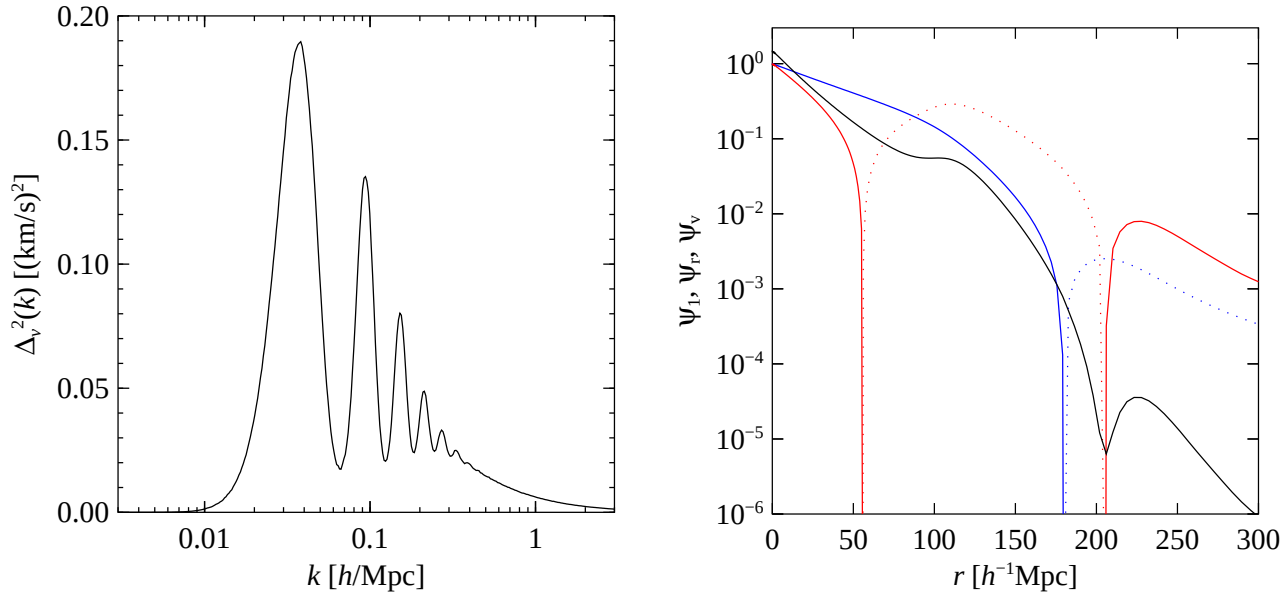

FIG. 1.— (Left) The power spectrum of v_{cb} fluctuations, $\Delta_v^2(k) = P_{\rm pri}(k)[a\dot{T}(k)]^2/2\pi^2 k$, at $z = 15$. (Right) Velocity correlation functions ψ_1 (blue), $\psi_r = \psi_1 + \psi_2$ (red), and $\psi_v = \psi_1^2 + \psi_r^2/2$ (black). Dotted curves depict regions where the correlation function is negative.

$$= -i\frac{a\boldsymbol{k}}{k^2}\dot{T}(\boldsymbol{k}, a)\delta_{\rm pri}(\boldsymbol{k}). \tag{4}$$

For adiabatic perturbations, CDM and baryons have the same primordial overdensity perturbations $\delta_{\rm pri}$, so the relative velocity is

$$\boldsymbol{v}_{cb}(\boldsymbol{k}, a) = -i\frac{a\boldsymbol{k}}{k^2}\dot{T}_{cb}(\boldsymbol{k}, a)\delta_{\rm pri}(\boldsymbol{k}), \tag{5}$$

where $T_{cb} = T_c - T_b$ is the difference between the CDM and baryon transfer functions. The two-point correlation function for velocities is then

$$\langle v_i(\boldsymbol{x})v_j(\boldsymbol{x}+\boldsymbol{r})\rangle = \sigma_1^2\left(\psi_1(r)\delta_{ij} + \psi_2(r)\frac{r_i r_j}{r^2}\right) \tag{6}$$

where

$$\sigma_1^2 = \frac{1}{3}\int \frac{P_{\rm pri}(k)[a\dot{T}]^2}{2\pi^2}dk \tag{7}$$

$$\psi_1(r) = \frac{1}{\sigma_1^2}\int \frac{P_{\rm pri}(k)[a\dot{T}]^2}{2\pi^2}\frac{j_1(kr)}{kr}dk \tag{8}$$

$$\psi_2(r) = -\frac{1}{\sigma_1^2}\int \frac{P_{\rm pri}(k)[a\dot{T}]^2}{2\pi^2}j_2(kr). \tag{9}$$

Here, $P_{\rm pri}(k)$ is the primordial density power spectrum, $\langle\delta_{\rm pri}(\boldsymbol{k}_1)\delta_{\rm pri}(\boldsymbol{k}_2)\rangle = (2\pi)^3 P_{\rm pri}(k_1)\delta^{(3)}(\boldsymbol{k}_1 + \boldsymbol{k}_2)$. Note that $P_{\rm pri}(k) = Ak^{n_s}$ is time-independent; all of the time dependence of the power spectrum is contained in the transfer function. We calculate the time-dependent CDM and baryon transfer functions using CAMB (Lewis et al. 2000). Figure 1 illustrates these velocity correlations. On small scales, velocities at nearby points are almost perfectly correlated, $\psi_1 \simeq 1$ and $\psi_2 \approx 0$. Towards larger scales of order the sound horizon ~ 150 Mpc, the radial component of the velocity is anti-correlated, since the relative CDM-baryon velocities are sourced by structures on these scales. The correlations fall off steeply on scales much larger than the sound horizon.

Since we have assumed that the collapse fraction f_c is a function of the local (relative) velocity $\boldsymbol{v}$, we can easily compute the probability distribution of f_c and its moments by integrating over the Gaussian distribution of $\boldsymbol{v}$. For example, the mean collapse fraction is

$$\langle f_c\rangle = \int P(\boldsymbol{v})f_c(v)d^3\boldsymbol{v} = \sqrt{\frac{2}{\pi}}\int f_c(v)e^{-v^2/2\sigma_1^2}\frac{v^2 dv}{\sigma_1^3}. \tag{10}$$

We plot the redshift dependence of $\langle f_c\rangle$ in Fig. 2.

Similarly, the two-point correlation function of f_c is

$$\langle f_c(x)f_c(x+r)\rangle = \int d^3\boldsymbol{v}_1 d^3\boldsymbol{v}_2 P(\boldsymbol{v}_1, \boldsymbol{v}_2)f_c(v_1)f_c(v_2) \tag{11}$$

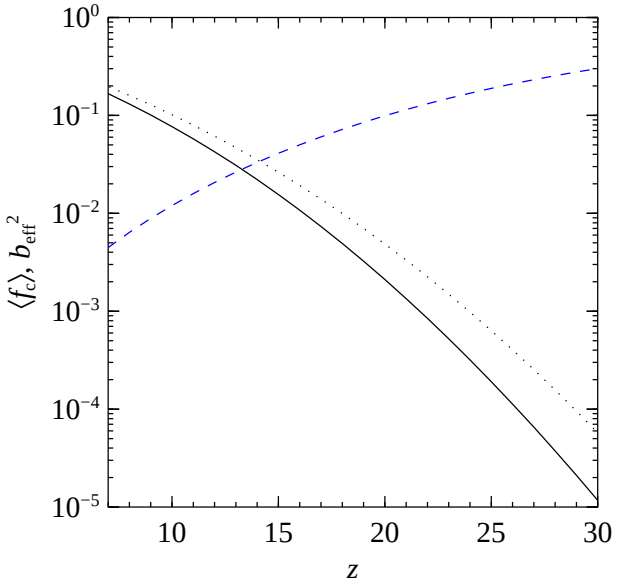

FIG. 2.— Redshift dependence of the mean collapse fraction $\langle f_c \rangle$ (solid black curve), the collapse fraction in the absence of relative baryon-DM motions $f_c(v=0)$ (dotted black curve), and the square of the effective bias, $b_{\rm eff}^2$ (dashed blue curve), defined in Eqn. (14).

where $\boldsymbol{v}_1$ and $\boldsymbol{v}_2$ are the velocities at points $\boldsymbol{x}$ and $\boldsymbol{x}+\boldsymbol{r}$, respectively, whose probability P is a Gaussian distribution with covariance given by Eqn. (6). This is a 6-D integral, however two of the integrals are elementary. If we write $\boldsymbol{u} = \boldsymbol{v}/\sigma_1$ with components u_r and u_t parallel and perpendicular to the separation vector, then

$$\langle f_c(x) f_c(x+r)\rangle = \int \frac{du_{1r}du_{2r}du_{1t}du_{2t}}{2\pi(1-\psi_1^2)(1-\psi_r^2)^{1/2}} f_c(v_1) f_c(v_2) u_{1t}u_{2t} I_0\left(\frac{\psi_1 u_{1t}u_{2t}}{1-\psi_1^2}\right) \times \exp\left(-\frac{1}{2}\left[\frac{u_{1t}^2+u_{2t}^2}{1-\psi_1^2} + \frac{u_{1r}^2+u_{2r}^2-2\psi_r u_{1r}u_{2r}}{1-\psi_r^2}\right]\right), \quad (12)$$

where $\psi_r = \psi_1 + \psi_2$ and $I_0(x)$ is a modified Bessel function. In various regimes, this integral may be simplified by Taylor expansion. For example, at large radius where $|\psi_1| \ll 1$ and $|\psi_r| \ll 1$, the two-point function is approximately

$$\langle f_c(x) f_c(x+r)\rangle \approx \frac{2}{\pi}\int du_1 du_2 u_1^2 u_2^2 f_c(v_1) f_c(v_2) e^{-(u_1^2+u_2^2)/2} \times \left[1 + \left(\psi_1^2 + \frac{\psi_r^2}{2}\right)\left(1 - \frac{u_1^2+u_2^2}{3} + \frac{u_1^2 u_2^2}{9}\right)\right]. \quad (13)$$

Writing $1 + \xi_f(r) = \langle f_c(x) f_c(x+r)\rangle / \langle f_c\rangle^2$, we find

$$\xi_f(r) \simeq \left(\psi_1^2 + \frac{\psi_r^2}{2}\right)\left(1 - \frac{\langle v^2 f_c\rangle}{\sigma^2\langle f_c\rangle}\right)^2 \equiv b_{\rm eff}^2\left(\psi_1^2 + \frac{\psi_r^2}{2}\right), \quad (14)$$

where $\sigma^2 = \langle v^2\rangle = 3\sigma_1^2$ is the 3-D velocity dispersion.

This expression has a straightforward interpretation. We have assumed that the collapse fraction is a function of the local velocity v. Therefore, on large scales, f_c will be a biased tracer of v^2. The two-point correlation function of v^2 is simply $2\psi_1^2 + \psi_r^2$. So Eqn. (14) is not surprising: f_c is indeed a biased tracer of v^2, with a large-scale bias coefficient $b_{\rm eff} = \langle v^2 f_c\rangle/\sigma^2\langle f_c\rangle - 1$. The form of this result is therefore generic. The numerical value of the bias coefficient depends on the precise details of the baryon content of low-mass halos, which we have assumed to be a step-function at M_c for simplicity. A more realistic model will have a slightly different bias coefficient, but the result that $\xi_f \propto \psi_v$ holds generically as long as the gas content of halos depends on the local relative bulk velocity.

In Figure 3 we plot the two-point correlation function and power spectrum of the baryonic collapse fraction. The two-point function exhibits strong clustering on large scales, roughly $\sim 10\%$ fractional fluctuations on 100 Mpc scales at $z = 20$. There is also a pronounced baryon acoustic oscillation feature, which is more plainly visible in the power spectrum. For comparison, we have also plotted the matter power spectrum at the same redshift. Two aspects to note are that the collapse fraction has considerably enhanced power on large scales, compared to the matter power spectrum, and that the amplitude of the baryon oscillations are far larger in the f_c power spectrum. As the figure illustrates, the baryon wiggles are typically percent level in the matter $P(k)$, while in the f_c power spectrum, the baryon oscillations are order unity.

3. LYMAN α PUMPING

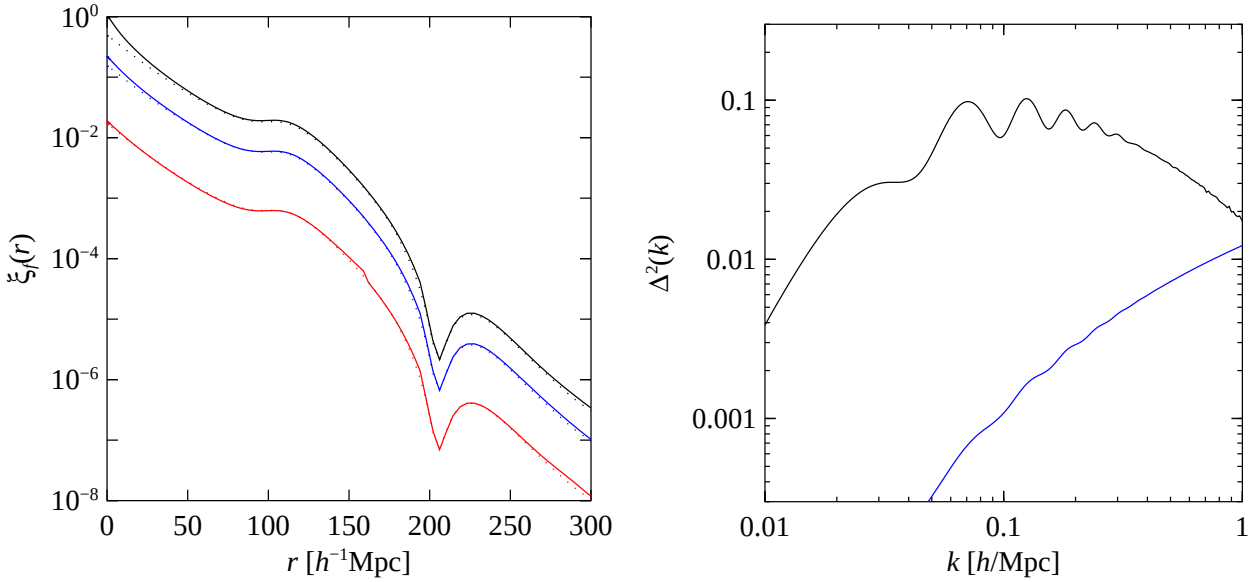

FIG. 3.— (Left) The f_c correlation function $\xi_f(r)$ at $z = 10$ (red), $z = 20$ (blue) and $z = 30$ (black). The solid curves show the full correlation function calculated from Eqn. (12), while the dotted curves show the linear bias approximation of Eqn. (14). At small radii, the linear bias approximation begins to break down, when Poisson-like clustering can become significant. (Right) The dimensionless power spectrum $\Delta^2 = k^3P(k)/2\pi^2$ for fractional fluctuations in collapse fraction $\delta_f = f_c/\langle f_c\rangle - 1$ (black) and matter $\delta = \rho/\bar{\rho} - 1$ (blue) at $z = 20$.

The large-scale modulations of collapsed baryonic mass found in the previous section can have several observable consequences. In this section, we discuss one such consequence: the effect of relative baryon-DM velocities on the 21-cm anisotropies preceding reionization. The physics of 21-cm fluctuations at high redshift has been discussed extensively in the literature; see Madau et al. (1997) and Furlanetto et al. (2006) for reviews.

Prior to reionization, the gas kinetic temperature $T_{\rm kin}$ is far below the CMB temperature: roughly speaking, $T_{\rm kin} \sim T_{\rm cmb} \times (1+z)/150$ for $z < 100$. When the first stars begin to emit Lyman-α radiation, the Wouthuysen-Field effect couples the spin temperature of neutral hydrogen atoms to the gas kinetic temperature, allowing neutral gas to be seen in 21-cm absorption against the cosmic microwave background. Neglecting atomic collisions, the spin temperature is given by

$$T_s^{-1} = \frac{T_{\rm cmb}^{-1} + x_\alpha T_{\rm kin}^{-1}}{1 + x_\alpha} \tag{15}$$

where the coupling coefficient x_α may be expressed in terms of the ratio of Lyman α photons to H atoms, n_α, as (Furlanetto et al. 2006)

$$x_\alpha = S_\alpha \frac{n_\alpha}{0.0767}\left(\frac{1+z}{20}\right)^2 \tag{16}$$

$$S_\alpha \approx \exp\left(-0.803 T_{\rm kin}^{-2/3}[\gamma \times 10^6]^{-1/3}\right) \tag{17}$$

$$\gamma = \frac{H}{\lambda_\alpha \sigma_\alpha n_{\rm H\,I}} \sim 3 \times 10^{-6} \frac{\Omega_m^{1/2}}{\Omega_b h (1+z)^{3/2}}. \tag{18}$$

Given the spin temperature T_s, the optical depth to 21 cm absorption is (Madau et al. 1997)

$$\tau = \frac{3c^3 h n_{\rm H\,I} A_{10}}{32\pi H \nu_0^2 k_B T_s} \approx 0.155 h \frac{\Omega_b}{\Omega_m^{1/2}} (1+z)^{3/2} x_{\rm H\,I} \left(\frac{T_s}{\rm K}\right)^{-1}, \tag{19}$$

and the observed (i.e. redshifted) 21 cm brightness temperature contrast against the CMB is then

$$\delta T_b = \frac{T_s - T_{\rm CMB}(z)}{1+z}(1 - e^{-\tau}), \tag{20}$$

where $T_{\rm CMB}(z) = 2.726(1+z)$ K. Therefore, given the Lyman-α intensity at any given point, we can compute the observed temperature contrast.

We estimate the Lyman α intensity by assuming that, on average, each collapsed baryon emits N_α Lyman α photons that escape into the intergalactic medium. For simplicity, we assume that photons are emitted with a flat spectrum, $\nu dN/d\nu = $const, but it is straightforward to generalize our results for an arbitrary emission spectrum. The local Lyman-α photon number density at each point in space and redshift is then given by a convolution of the collapsed

baryon density with a retarded Green's function,

$$n_\alpha = N_\alpha \int d^3r\, d\eta \frac{df_c}{d\eta}(\boldsymbol{r},\eta)\frac{\delta(\eta + r/c)}{4\pi r^2 c}, \tag{21}$$

or in Fourier space,

$$n_\alpha(\boldsymbol{k},\eta_0) = N_\alpha \int_0^{\eta_0} d\eta \frac{df_c}{d\eta}(\boldsymbol{k},\eta) j_0(kc(\eta_0-\eta)) \tag{22}$$

where η is conformal time and $j_0(x) = \sin(x)/x$. We can further simplify this expression by using our previous result that, on large scales, $f_c(\boldsymbol{k})$ has time dependence $\propto \langle f_c\rangle b_{\rm eff} = \langle f_c\rangle - \langle v^2 f_c\rangle/\sigma^2$. Therefore, we have

$$n_\alpha(\boldsymbol{k},z) = N_\alpha f_c(\boldsymbol{k},z) W(k,z) \tag{23}$$

where the smoothing filter is

$$W(k,z) = \frac{1}{\langle f_c\rangle b_{\rm eff}} \int_0^{\eta_0} d\eta \frac{d\langle f_c\rangle b_{\rm eff}}{d\eta} j_0(kc(\eta_0-\eta)). \tag{24}$$

In this expression, η_0 is the conformal time at redshift z, and note that $d/d\eta = -H\, d/dz$.

The propagation of Lyman α photons over large distances considerably damps the spatial fluctuations in Ly α intensity. However, our discussion so far has neglected an important effect: Lyman α photons can only travel a limited distance. A rest frame Lyman α photon which participates in pumping was emitted at some distance bluewards of Lyman α, redshifting as it travels. The higher the frequency at emission, the longer the distance that the photon travels before redshifting into Lyman α. However, a photon that is emitted at a wavelength shorter than Lyman β will be absorbed in the neutral intergalactic medium, and ultimately lost to double photon decay, before it can redshift into Lyman α. This means that gas clouds at redshift z cannot be pumped by photons emitted by sources at redshift $z_{\rm emit} > z_{\rm hor}$, where $(1+z_{\rm hor}) = (32/27)\times(1+z)$. This gives a natural maximal horizon distance for Lyman α pumping. Conceivably, the propagation distance could be even shorter given sufficient molecular opacity, either in the host minihalos or in the intergalactic medium (Ricotti et al. 2001), but we disregard this possibility in our calculations.

If $z_{\rm hor}/z - 1 \ll 1$, we can approximate Eqn. (24) as

$$W(k,z) \approx -\frac{1}{\langle f_c\rangle b_{\rm eff}} \int_z^{z_{\rm hor}} dz_e \frac{d\langle f_c\rangle b_{\rm eff}}{dz} j_0\left(\frac{kc}{H}(z_e - z)\right). \tag{25}$$

This shows how the shape of the smoothing window depends on the formation history of collapsed baryonic objects and their Lyman α emission. As noted above, the shape of $W(k,z)$ also depends on the spectrum of escaping UV emission from the first stars, which will generally be much more complicated than we have assumed here. Fortunately, it is entirely straightforward to compute how W changes when realistic spectra and opacity are used instead of the flat spectrum and sharp cutoff that we have adopted for simplicity. Given this expression for the smoothing window, we can compute the number of Lyman α photons per atom, n_α, using Eqn. (23), which then gives x_α and the spin temperature T_s using Eqns. (15-16). Given T_s, we compute the optical depth and brightness temperature using Eqns. (19-20).

The Lyman-α intensity n_α is a linear function of the collapse fraction, so its power spectrum is simply the product of the f_c power spectrum with the (square of the) window function, Eqn. (24). The brightness temperature is a nonlinear but local function of n_α. Therefore, on large scales it is a biased tracer of the intensity field, and its power spectrum will be proportional to the n_α power spectrum, with some proportionality coefficient. We could write down an analytic expression for this bias coefficient in terms of the N-point correlation functions of n_α, but it is simpler to calculate it by simulation instead. Accordingly, we have generated realizations of the brightness temperature field. We first generate realizations of the Gaussian random relative velocity field v_{cb}, which we then transform into collapse fraction f_c using Eqns. (1-2), replacing $c_s \to c_{s,\rm eff}$ as described in §2. From the collapse fraction, we compute the Lyman-α intensity using Eqn. (23), which then gives the spin temperature T_s, optical depth τ and brightness temperature contrast δT_b using Eqns. (15-20). We generate realizations in a 2 h^{-1}Gpc box of 1024^3 pixels at a variety of different redshifts, varying the number of Lyman-α photons per collapsed baryon, N_α.

Figure 4 illustrates the brightness temperature power spectrum. As expected, the δT_b power spectrum is proportional to the product of the f_c power spectrum, multiplied by the square of the window function $W(k,z)$ given by Eqn. (24), which suppresses small-scale fluctuations in the brightness temperature. The shape of the power spectrum is therefore simple to calculate. The power spectrum peaks on the scale of the Lyman-α horizon, and exhibits damped but pronounced acoustic oscillations at higher wavevectors.

The amplitude of the power spectrum is a nontrivial function of N_α and z. At high redshift, when the collapse fraction is small and the Lyman-α pumping intensity n_α is weak, the spin temperature is close to the CMB temperature, with small fluctuations proportional to n_α. The brightness temperature contrast therefore grows rapidly in time. Eventually, however, the spin temperature begins to saturate at the gas kinetic temperature $T_{\rm kin}$. As n_α becomes very large, the spin temperature begins to approach a uniform value everywhere, $T_s \to T_{\rm kin}$, and so the brightness temperature fluctuations actually diminish with increasing n_α. Accordingly, the δT_b power spectrum peaks and then decreases towards lower redshift. Of course, our assumption that $T_{\rm kin}$ remains close to its adiabatic value becomes suspect in

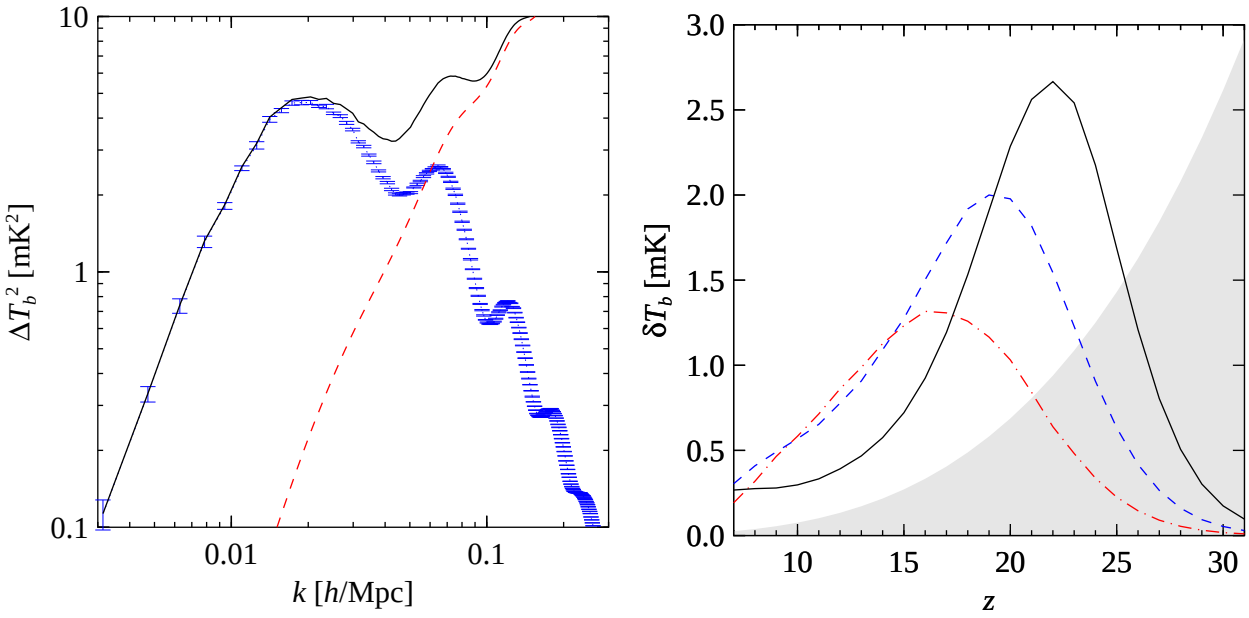

FIG. 4.— (Left) The 21 cm temperature power spectrum at redshift $z = 20$, for $N_\alpha = 100$ Lyman α photons per collapsed atom. The blue curve with error bars shows the brightness power spectrum from UV sources that trace minihalos, while the red dashed curve shows the fluctuations expected for uniform Lyman α radiation that pumps gas with density fluctuations tracing the matter density fluctuations at this redshift. Since density and velocity are uncorrelated, these two power spectra add linearly (solid black curve). (Right) RMS temperature fluctuations δT_b as a function of redshift z for a Gaussian beam with a diffraction limit of a 500m dish (such as FAST). A 300m dish measures a slightly lower signal. Different curves are: $N_\alpha = 10$ (red dot-dash), 30 (blue dashed) and 100 (black solid). The shaded area indicates the $1-\sigma$ errors per unit redshift expected for 1000 days of observations using a 500m dish like FAST.

this regime. Eventually, a sufficiently strong Lyman-α intensity will not merely pump the 21-cm transition, but will appreciably heat the gas as well.

4. OBSERVATIONAL PROSPECTS

In order to measure the very large scale structure, one needs high brightness sensitivity on BAO scales. At $z > 10$, the angular scale of BAO changes little, and $\sim 10'$ scales are important, just as they are in the CMB.

To achieve high brightness sensitivity, a filled aperture is desirable. Telescopes such as Arecibo and FAST (Smits et al. 2009) would be well suited. With filled apertures of 300m and 500m respectively, their angular resolution for 21 cm at $z \sim 20$ is 40 and 30 arc minutes, respectively. We focus our attention on FAST, which is expected to observe at sufficiently long wavelengths. At these low frequencies, sensitivities are sky limited, with $T_{\rm sys} \sim 3000$K. It is also straightforward to observe with a focal plane array, so we reference our forecasts to a 100 pixel array, which would be a 40m dipole array. Such a focal plane array would allow primary beam illumination to compensate with frequency to make frequency independent beams, enabling accurate foreground subtraction. The maximum transverse $k_\perp = 0.08$.

We further assume the sky is drift scanned, which minimizes systematic errors, and makes this experiment comparable to the recent GBT 21cm intensity detection (Chang et al. 2010). For a square array, the field of view is 10 beam width, or about 5 degrees. We use half the scanned area as useful, allowing for galaxy and point source cuts.

At zenith for a latitude of 30 degrees, this scans 1000 square degrees. We use an integration time of 1000 days on the sky. The exposure time per pixel is 5×10^6 seconds. In a bandwidth of 2 MHz, this results in a pixel noise of 1 mK, well matched to the expected signal. This map contains $\sim 10^5$ pixels, so one expects to measure the power on the beam scale with $\sim 100\sigma$.

The specific forecast parameters used for the noise estimate in figure 4 are: $T_{\rm sky} = 300(\nu/150{\rm MHz})^{-2.7}$, 24 beams on the sky (the equivalent of a LOFAR station signal processor), and a diffraction limited beam.

5. DISCUSSION

We have investigated the effect of relative motions between baryons and dark matter on the formation of the smallest galaxies at high redshift, $z \sim 20$. The formation of galaxies in minihalos of mass $M \lesssim 10^6 M_\odot$ is modulated by large-scale bulk velocities between gas and dark matter, and so the clustering of these objects will contain a contribution proportional to the relative velocity two-point function. The velocity power spectrum exhibits significant correlations on large scales of order 100 Mpc, with pronounced baryon acoustic oscillations. Accordingly, the large-scale clustering of minihalos exhibits similar features, and the large-scale correlations of any observable that traces minihalos will show similar behavior. We illustrated this in the previous section with a calculation of the 21 cm absorption power spectrum prior to reionization, when the kinetic temperature of intergalactic gas is much colder than the CMB temperature. Our predictions for 21 cm absorption are model dependent, principally depending on the number of Lyman α photons emitted per collapsed baryon.

A similar argument holds for any observable that traces minihalos. For example, suppose that minihalos make a significant contribution to the ionizing flux at the time of reionization. Then the large-scale power spectrum of

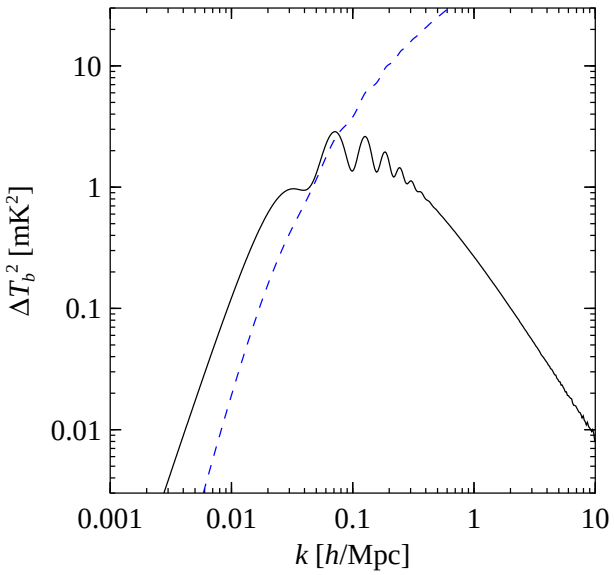

FIG. 5.— The 21 cm temperature power spectrum $\Delta T_b^2 = k^3 P(k)/2\pi^2$ at $z = 10$ (solid black), assuming that the ionized fraction is proportional to the local baryon collapsed fraction, $x_e \propto f_c$. For comparison, we also plot the matter power spectrum multiplied by $(1+z) \times (9.4\text{mK})^2$, as the dotted blue curve.

patchy reionization will contain a contribution proportional to the bulk velocity power spectrum, as can easily be seen. During reionization, let us assume that $T_s \gg T_{\rm CMB}$, and that fluctuations in the ionized fraction x_e trace the local collapsed fraction f_c. In this regime, the observed temperature contrast in Eqn. (20) becomes independent of the spin temperature

$$\delta T_b \simeq 0.155\text{K}\ h \frac{\Omega_b}{\Omega_m^{1/2}} (1+z)^{1/2} x_e \approx 9.4\text{mK}\,(1+z)^{1/2} x_e. \tag{26}$$

We fix the proportionality constant relating x_e and f_c by requiring that the Thomson scattering optical depth τ cannot exceed the WMAP bound, $\tau = 0.088$. We assume that reionization completes at $z_{\rm re} = 7$, and assume that x_e at $z > z_{\rm re}$ is patchy and traces f_c. This provides an upper bound on the patchy reionization signal from minihalos. The resulting power spectrum is shown in Fig. 5. As expected, the minihalo contribution to the power spectrum shows pronounced baryon acoustic oscillations, which will be at least partially smoothed when we account for the $\sim 5-10$ Mpc sizes of ionized bubbles during reionization.

Although this signal could be present, detecting it during reionization may be challenging in practice, since there are other sources of large-scale power in 21-cm correlations. For example, the clustering of the ionizing sources will reflect the clustering of the halos hosting those sources, which trace the clustering of the matter field. Because matter density fluctuations are uncorrelated with bulk velocity fluctuations, these two terms simply add in the overall power spectrum of the sources. Realistically, we expect the clustering from bulk velocities to be subdominant to the clustering from density perturbations over many of the scales of interest during reionization (see Fig. 5). On the other hand, TH have shown that the halo power spectrum itself also contains a term proportional to the relative bulk velocity power spectrum, for halos of order $M \sim 10^6 M_\odot$.

Another place where these effects may be observable is in the CMB itself. At small angular scales, the so called kinetic Sunyaev-Zeldovich effect, caused by radial Doppler motions of electrons off which photons scatter, can be important (e.g. Hernández-Monteagudo & Ho 2009). This effect is enhanced if reionization is patchy (McQuinn et al. 2005). If these reionization patches have suppressed bulk velocities then the effect will be reduced. On the other hand, the large scale correlation of reionization patches predicted here will lead to large scale fluctuations in optical depth, inducing a modulated suppression of primary CMB fluctuations, which may be detectable with a higher order correlation analysis in CMB.

At low redshifts, $z \lesssim 5$, the typical masses of collapsing halos are generally much larger than minihalo masses, and so we would naively expect the effects of relative velocities between DM and baryons to become unimportant. However, in principle the signatures of minihalos could persist even in late-time observables. For example, if reionization is patchy on ~ 100 Mpc scales due to minihalos, the subsequent star formation history inside patches that reionize early could differ from patches that reionize later. This could lead to spatial variations in galaxy formation at late times, on scales of order the BAO scale. This is potentially worrisome for BAO probes of dark energy (e.g. Schlegel et al. 2009), which rely on precise determination of the BAO feature in the galaxy two-point function. Any contamination from minihalo effects could shift the location of the BAO feature and thereby create a bias in measurements of the equation of state parameter w, analogous to the results of Pritchard et al. (2007). Removing this source of systematic uncertainty appears daunting. Eisenstein et al. (2007) have shown that BAO probes of dark energy are quite insensitive to smooth distortions to the shape of the power spectrum. However, the minihalo effect could be far more pernicious, since the velocity power spectrum is not smooth, but has pronounced baryon oscillations that are presumably out of

phase with the oscillations in the matter power spectrum. Marginalizing over an unknown minihalo contaminant could significantly degrade BAO constraints on dark energy. This underscores the need for more work on this subject.

In summary, the supersonic relative motions between baryons and dark matter can dramatically affect the formation of the earliest collapsed baryonic objects in the Universe. We expect the abundance of minihalos of mass $M \sim 10^5 M_\odot$ to be modulated on ~ 100 Mpc scales, and any tracer of minihalos should show the same modulations, with highly pronounced baryon acoustic oscillations. Specific predictions for any observable are necessarily model dependent, but for plausible scenarios this large scale signal is within the sensitivity range of existing and upcoming observatories. This effect could allow us to detect the signature of the earliest galaxies, written across the sky.

We thank Chris Hirata for useful discussions. The calculations presented in this paper have made use of publicly available software, including CAMB[1], CUBA[2], FFTLog[3] and GSL[4]. We thank the authors of these libraries for making their software public. This work is supported by the Swiss National Foundation under contract 200021-116696/1 and WCU grant R32-2009-000-10130-0.

REFERENCES

Bromm, V., Yoshida, N., Hernquist, L., & McKee, C. F. 2009, Nature, 459, 49, arXiv:0905.0929
Chang, T., Pen, U., Bandura, K., & Peterson, J. B. 2010, Nature, 466, 463
Eisenstein, D. J., Seo, H., & White, M. 2007, ApJ, 664, 660, arXiv:astro-ph/0604361
Fan, X., Carilli, C. L., & Keating, B. 2006, ARA&A, 44, 415, arXiv:astro-ph/0602375
Furlanetto, S. R., Oh, S. P., & Briggs, F. H. 2006, Phys. Rep., 433, 181, arXiv:astro-ph/0608032
Gnedin, N. Y. 2000, ApJ, 542, 535, arXiv:astro-ph/0002151
Gnedin, N. Y., & Hui, L. 1998, MNRAS, 296, 44, arXiv:astro-ph/9706219
Green, A. M., Hofmann, S., & Schwarz, D. J. 2005, JCAP, 8, 3, arXiv:astro-ph/0503387
Hernández-Monteagudo, C., & Ho, S. 2009, MNRAS, 398, 790, arXiv:0903.2814
Larson, D. et al. 2010, arXiv:1001.4635
Lewis, A., Challinor, A., & Lasenby, A. 2000, ApJ, 538, 473, arXiv:astro-ph/9911177
Loeb, A. 2010, How did the first stars and galaxies form? (Princeton University Press)
Madau, P., Meiksin, A., & Rees, M. J. 1997, ApJ, 475, 429, arXiv:astro-ph/9608010
McQuinn, M., Furlanetto, S. R., Hernquist, L., Zahn, O., & Zaldarriaga, M. 2005, ApJ, 630, 643, arXiv:astro-ph/0504189
Naoz, S., Yoshida, N., & Barkana, R. 2010, arXiv:1009.0945
Pritchard, J. R., Furlanetto, S. R., & Kamionkowski, M. 2007, MNRAS, 374, 159, arXiv:astro-ph/0604358
Ricotti, M., Gnedin, N. Y., & Shull, J. M. 2001, ApJ, 560, 580, arXiv:astro-ph/0012335
Schlegel, D., White, M., & Eisenstein, D. 2009, in Astronomy, Vol. 2010, astro2010: The Astronomy and Astrophysics Decadal Survey, 314–+, arXiv:0902.4680
Sheth, R. K., Mo, H. J., & Tormen, G. 2001, MNRAS, 323, 1, arXiv:astro-ph/9907024
Smits, R., Lorimer, D. R., Kramer, M., Manchester, R., Stappers, B., Jin, C. J., Nan, R. D., & Li, D. 2009, A&A, 505, 919, arXiv:0908.1689
Tegmark, M., Silk, J., Rees, M. J., Blanchard, A., Abel, T., & Palla, F. 1997, ApJ, 474, 1, arXiv:astro-ph/9603007
Tseliakhovich, D., & Hirata, C. 2010, arXiv:1005.2416
Yoshida, N., Oh, S. P., Kitayama, T., & Hernquist, L. 2007, ApJ, 663, 687, arXiv:astro-ph/0610819

[1] http://camb.info
[2] http://www.feynarts.de/cuba
[3] http://casa.colorado.edu/∼ajsh/FFTLog
[4] http://www.gnu.org/software/gsl